ELSEVIER

Journal of Fluids and Structures 18 (2003) 425–440

JOURNAL OF FLUIDS AND STRUCTURES

www.elsevier.nl/locate/jnlabr/yjfls

Flow-induced vibration testing of replacement thermowell designs

K.H. Haslinger

Westinghouse Electric Company, 2000 Day Hill Road, Windsor, CT 06095, USA

Received 21 June 2002; accepted 18 July 2003

Abstract

Inconel 600 Primary Water Stress Corrosion Cracking (PWSCC) in Nuclear Pressurized Water Reactors (PWRs) has necessitated the repair/replacement of various small bore nozzles. These repairs/replacements must be designed to avoid unwanted vibrations. So, to this end, new RTD-Thermowell-Nozzle replacement designs were developed and subjected to flow testing over a velocity range from 9.14 to 33.53 m/s (30–110 ft/s), and temperatures ranging from 121°C to 316°C (250–600°F). The replacement nozzles are welded on the pipe OD, rather than on the pipe ID. A split, tapered ferrule is used to support the nozzle tip inside the pipe bore. This maintains high thermowell tip-resonance frequencies with the objective of avoiding self-excitation from vortex shedding that is believed to have caused failures in an earlier design during initial, precritical plant startup testing. The flow testing was complicated by the small size of the thermowell tips (5.08 mm or 0.2 in ID), which necessitated use of a complement of low temperature and high temperature instrumentation. Since the high temperature device had an internal resonance (750 Hz) within the frequency range of interest (0–2500 Hz), adequate sensor correlations had to be derived from low temperature tests. The current nozzle/thermowell design was tested concurrently with two slight variations of the replacement design. The acceleration signals were acquired during incremental and continuous flow sweeps, nominally at 5 kHz sampling rates and for time domain processing as high as 25 kHz. Whereas vortex-shedding frequencies were predicted to prevail between 400 and 1500 Hz, no such response was observed at these frequencies. Rather, the thermowell tips responded due to turbulent buffeting with a peak response that was related directly to flow velocity. Lift direction response was always larger than drag direction response. The thermowell tips also responded at their natural tip frequencies in a narrow band random fashion. At the higher flow rates, one replacement design experienced an instability mode leading to high tip stresses. Although this instability did not repeat, this particular design was eliminated from consideration. The second replacement design performed almost identically to the current in-plant design. The experimental data were used to extract forcing functions and thermowell responses that were used as input into the design calculations.

1. Introduction

Reliability of any replacement component in a nuclear plant is important. Prior to introducing a "new 3/4" Resistance Temperature Detector (RTD) replacement thermowell design, an extensive qualification program was performed in 2001. The term "new 3/4 " refers to a shortened nozzle length; the thermowell and the RTD remain at the original full length. Flow-induced vibration (FIV) testing of the new design, as well as of the current design, was pursued in order to simulate the "in-plant" flow conditions as reliably as possible, and to obtain all the design and thermowell flow response information needed for qualification of the replacement design. Based on previous thermowell failures during start-up operations, the major concern was excessive thermowell tip-resonance response due to vortex

E-mail address: karl.h.haslinger@us.westinghouse.com (K.H. Haslinger).

0889-9746/$ - see front matter © 2003 Elsevier Ltd. All rights reserved.
doi:10.1016/j.jfluidstructs.2003.07.012

Nomenclature

A	projected area of tube/thermowell tip (mm^2)
$C_{d,l}$	effective force coefficient, drag or lift (dimensionless)
D	diameter (mm)
F_A	force over area A (N)
f_n	natural frequency (Hz)
$f_s = SV/D$	vortex shedding frequency (Hz)
$f_r = f_n D/V_g$	reduced frequency (dimensionless)
g	gravitational constant (m/s^2)
L_c	generalized correlation length (mm)
l	length (mm)
M	generalized mass (kg)
m	mass per unit length, including added mass effects of fluid (kg/m)
n	subscript defining a particular mode
PSD	power spectral density
S	Strouhal number (dimensionless)
t	time (s)
V_g	average radial (gap) velocity (m/s)
$\delta(s)$	relative modal deflection at location s (dimensionless)
ζ	critical damping ratio (dimensionless)
ρ	fluid density (kg/m^3)
$\sigma(s)$	r.m.s. tube response at point s (mm)
ϕ_F	turbulence spectrum level at f_r (dimensionless)

shedding. Extensive vibration testing performed in 1983 subsequently led to the development of a tapered precision thermowell that has been in operation in several plants for almost 20 years. The basic design features and hydraulic performance of this original design are maintained by the 3/4 RTD replacement design, as demonstrated by the flow test program described in this article.

2. Test design

Incremental and continuous flow sweep type FIV testing of the current thermowell (reference design) and of two slight variations of a new thermowell replacement design was intended to investigate their responses due to vortex shedding up to design flow velocities of 33.53 m/s (110 ft/s). Due to instrumentation limitations, and also to investigate plant start-up conditions, testing was conducted at three different temperatures. The results from the testing were intended to assure acceptable FIV response of any selected replacement design, similar to that demonstrated by the current in-plant design. Also, the test results were to be used directly as input for the design stress analyses for the RTD chosen by the plant. Collateral testing activities, not described in this article, dealt with replacement hardware installation techniques and mechanical or thermal cycling of the 3/4 design nozzle tip support features in order to demonstrate their reliable long-term support function in the plant. Also, because Inconel 690 (versus type 600) replacement material is used for both nozzles and thermowells, a series of successful RTD response time tests were performed at simulated plant design conditions. The hydraulic qualification testing of the 3/4 RTD design was the last test program conducted in the Westinghouse TF-2 test loop prior to its decommissioning.

2.1. Test facility

Qualification tests on reactor components, including full-scale prototype fuel designs, were performed until the fall of 2001 in the Westinghouse TF-2 test facility, as shown schematically in Fig. 1a. This test loop was recently decommissioned and was replaced by the VIPER test loop located in Columbia, SC. The TF-2 test loop was constructed of stainless steel and was designed for flow rates up to 3400 m^3/h (15,000 gpm), temperatures up to 343°C (650°F), and pressures up to 17.24 MPa (2500 psi). The loop had two test-sections, a 915 mm (36 in) diameter main

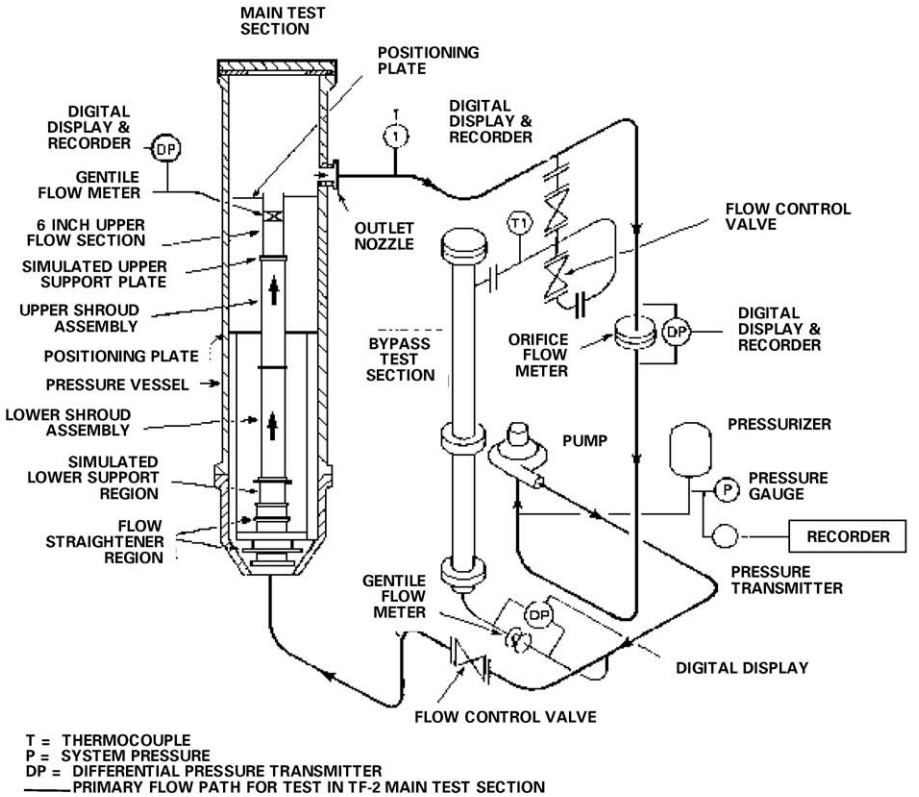

(a)

(b)

Fig. 1. (a) TF-2 test loop schematic, (b) photograph of test-section exiting TF-2 outlet nozzle.

test-section and a smaller diameter by-pass section. The outlet nozzle of the main test-section was used for the subject tests. A single stage pump, which could be operated at two speeds, provided the energy input to the test loop. Test-section flow was monitored by an orifice type flow meter, located in the pump outlet section.

2.2. Thermowell/RTD/nozzle designs

Fig. 2 shows the installation of the new 3/4 RTD replacement nozzle design in a 101.6 mm (4 in) thick section of a hot leg pipe. In the 3/4-nozzle technique, the current Alloy 600 nozzles are cut outboard of the J-groove partial penetration welds that are between the Alloy 600 nozzles and the carbon steel pipe. This part of the Alloy 600 nozzle is replaced with a shortened nozzle (3/4-nozzle) of Alloy 690 that is welded to the pipe outside diameter. The original J-groove welds and short sections of the Alloy 600 nozzles remain in place. Further, there are gaps of approximately 3.2 mm (1/8 in) between the new nozzle tips and the remnants of the old Alloy 600 nozzles. The Version B design had a 19 mm (3/4 in) thick remnant compared with the 6.35 mm (1/4 in) thick remnant of the Version A design. The thicker remnant would have kept the ferrule (see below) outside the original J-Weld zone. However, the longer free tip resulted in lower tip frequencies. The replacement nozzles are tapered at the in-board end and the tapered end has 24 narrow splines. The tapered end is forced into a split ring (ferrule) with internal taper and small undercut on the backside. Fig. 3 shows the details of these components. The purpose of the ferrule is to provide a tip support close to the pipe ID, thus maintaining high thermowell/nozzle tip-resonance frequencies to avoid any complications from FIVs. A counterbore in the pipe increases the diameter of the hole by 1.5 mm (0.060 in) over much of its length. A shoulder in the pipe bore is thus created that is 0.75 mm (0.030 in) in width, against which the split ring rests. The shoulder is strong enough to resist any

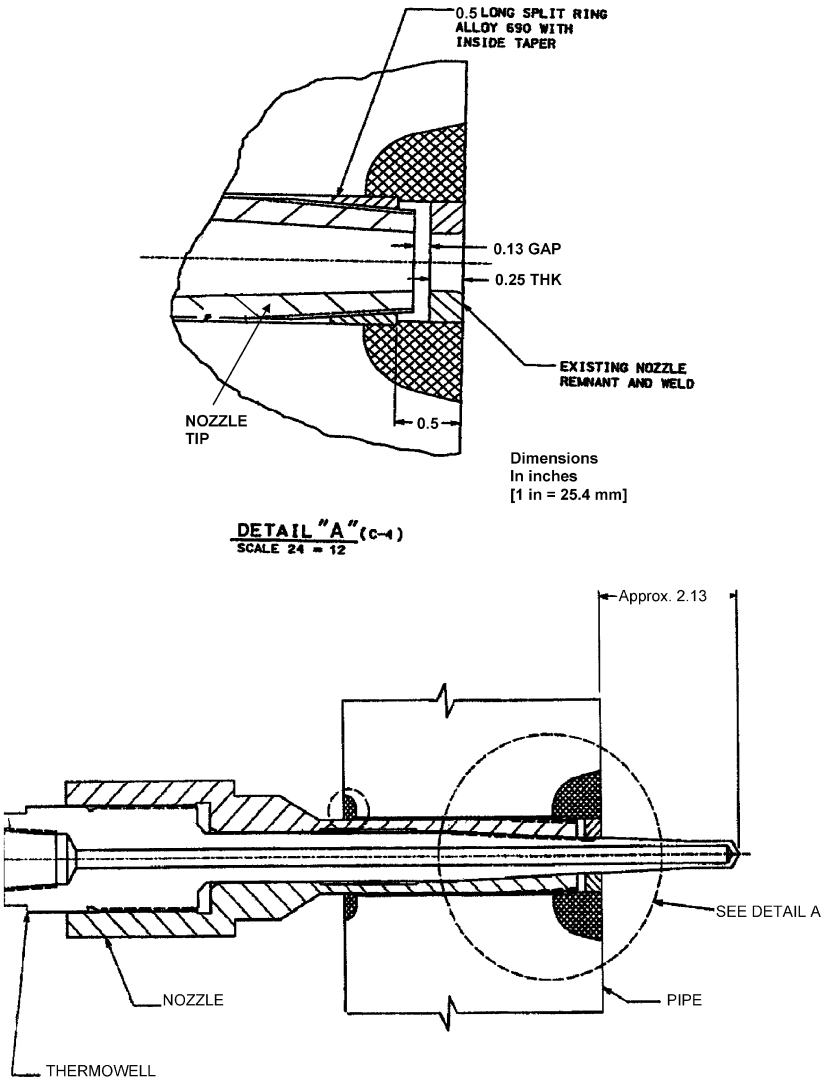

Fig. 2. 3/4 thermowell nozzle replacement design sketches.

longitudinal forces due to thermal growth differences between the nozzle and pipe. The interface between the nozzle splines and the tapered ferrule ID is designed such that it will permit small axial movements without loss of the lateral support restraint. The undercut on the backside of the ferrule provides an elastic support feature that, in addition to the plastically created support grooves (during installation process), will assure adequate tip support over the lifetime of the plants. The design features of the "ferrule-to-pipe-bore" contact region address long-term corrosion issues and prevent aggravated growth of any residual cracks in the original J-welds. In order to assure long term support effectiveness from the ferrule/spline interface, the test-section was thermal-cycled to the equivalent of in-plant exposure and the support function was shown to be unimpaired, based on unchanged tip-resonance frequencies.

2.3. Test-section

The flow test assembly consisted of a 1.34 m (52.75 in) long inlet flow tube, a special flange assembly that housed the three RTD nozzles, and of a 1.06 m (41.75 in) long outlet flow tube. The flow tubes were fabricated of 152 mm (6 in) Schedule 160 carbon steel pipe with a 133.3-mm (5.250-in) machined ID dimension. Fig. 4 shows various details of this flow test arrangement. The central flange section was sandwiched between the 406-mm (16-in) flanges of the TF-2 main test-section outlet nozzle. Fig. 1b shows the test-section during installation. The flow tube lengths were designed to provide ten straight upstream and eight straight downstream diameters relative to the thermowell location. All three thermowell nozzles were placed in 90° increments at the center plane of the test-section and, thus, were tested simultaneously. However, there was sufficient spacing between the nozzle tips to avoid any significant interaction. The projected area of all three nozzle tips was 17.87 cm^2 (2.77 in^2), which represents about a 12.8% flow obstruction of the total flow tube cross-section of 139.6 cm^2 (21.64 in^2).

2.4. Test instrumentation

The test-section itself was instrumented with accelerometers to monitor its vibratory response behavior with respect to the drag (flow direction) and all lift directions of the thermowell tips. Additional accelerometers were installed at the RTD heads. Each of the three thermowell tips was instrumented with biaxial accelerometer installations. For this purpose, thin wall tubing was used to simulate the RTDs and their mounting inside the thermowells. Both low temperature and high temperature micro-miniature accelerometers were commercially available for monitoring the actual tip motions. The low temperature Endevco devices had been used in the early 1980s for a similar test program, but did not survive temperatures higher than 150°C (302°F). The hermetically sealed Vibrometer biaxial accelerometer offers high temperature performance. However, this design has an internal resonance near 1000 Hz, within the frequency range of interest (from 0 to 2500 Hz). No other instrumentation was readily available and the decision was made to perform extensive comparative testing at low temperature with the objective of establishing adequate sensor correlations that would allow use of the Vibrometer accelerometer at "high" temperature test environments. An intermediate test temperature of 232°C (450°F) was chosen in order to have a transition region where both devices were still operational.

2.5. Flow sweep test

The design flow rates for the hot leg and the cold leg of a particular nuclear power plant are (25.6 m/s) 84 ft/s and 33.53 m/s (110 ft/s) velocity, respectively. Actual operating velocities are approximately 20% lower. In order to capture any potential FIV responses of the thermowell designs over a very broad range of operating conditions, incremental and continuous flow sweep test cycles were conducted from 9.1 to 33.5 m/s (30–110 ft/s) and loop conditions of 121°C, 232°C and 316°C (250°F, 450°F and 600°F). The initial focus was on the detection of any response due to Vortex shedding excitation that, with increase in flow velocity, was expected to traverse a frequency range of approximately 400–1600 Hz. The incremental testing permitted the acquisition of "steady state" data and full processing of data-channel interrelated information. The continuous flow sweep method permitted the display of response data that were acquired in 30-min time intervals over the entire sweep range.

2.6. Data acquisition

Transient and steady state vibration data were acquired via a 64-channel capacity data acquisition system. Each data channel was sampled at 5000 samples per second in order to provide the desired resolution in the frequency domain up to 2500 Hz. Selected acquisition runs were performed using 25,000 samples per second to allow reprocessing of results in the time domain. The test-signals were viewed and analyzed in real time on monitors and spectrum analyzers. The

Fig. 3. Photograph of 3/4 thermowell nozzle design.

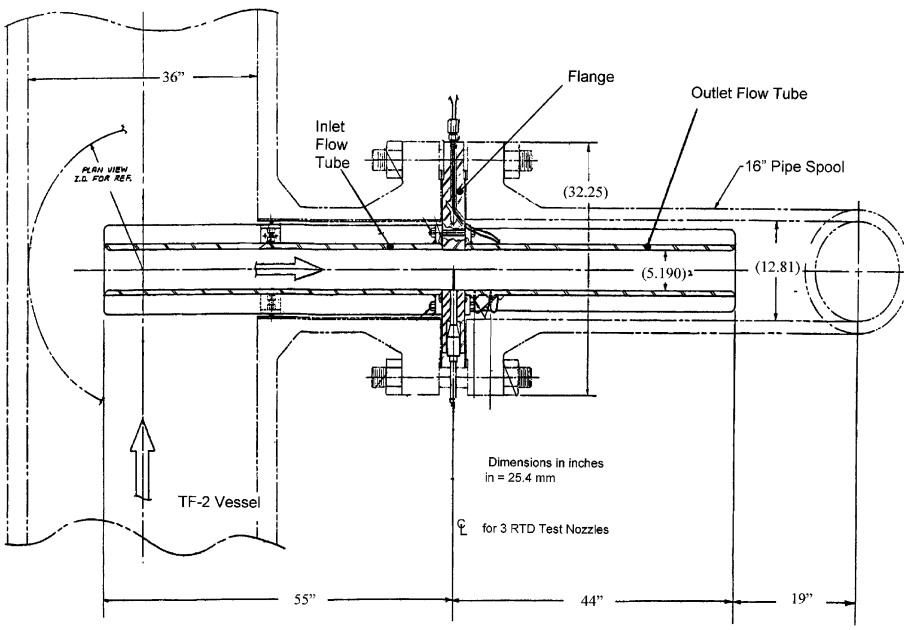

Fig. 4. RTD test-section in TF-2 outlet nozzle/pipe.

Westinghouse Darwin computer program was used for final processing of results in terms of PSD, Phase, Coherence, Time History, and Transfer Function plots, as well as the creation of Waterfall graphs. Spreadsheet templates were used to display time synchronized orbital motions and time history collages, which included double integration of accelerometer signals to provide displacement motion graphs.

3. Test results

3.1. General observations and data adjustments

The first set of acceleration spectra for the low temperature test condition provided no evidence of any vortex shedding response. Rather, it revealed very contrasting spectrum profiles generated by the two different types of accelerometer sensors. Referring to Fig. 5a (where the term "unit" is in "Gs"), the Endevco accelerometer spectra were dominated by a high-frequency peak (at 2000 Hz and above) that was attributed to the thermowell tip resonance. The Vibrometer accelerometer spectra were dominated by a bias 750–1000 Hz peak that was easily attributed to the accelerometer's internal resonance behavior. The Vibrometer spectra also revealed the thermowell tip-resonance peaks, however at a much-attenuated level. Fig. 5b shows both lift axis and drag acceleration spectra for the 3/4 Version A design. The correct (Endevco) spectrum profile is shown superimposed, along with the terminology chosen to describe the various response regions and accelerometer performances. Since the tip stress magnitudes are controlled by the tip deflection, rather than by the tip acceleration, all spectra were double integrated in the frequency domain to represent tip deflections in terms of "mils". This presentation method, Fig. 6, allowed detection of a more significant level of "turbulent buffeting"[1] response that was evident within a frequency range as wide as 75–600 Hz. Below 100 Hz, the signal peaks were attributed to instrumentation noise. There were cases where strong high-frequency response motions, due to signal aliasing, created very significant low-frequency bias peaks that needed to be ignored completely. In order to deal with the large disparity in the sensor output behavior, it could be assumed that the low temperature Endevco accelerometers, with internal resonances well above 10 kHz, are reliable devices. The test data from the Vibrometer accelerometer confirmed its internal resonance at 750 Hz with an amplification factor of 35. Using the response function for a single degree of freedom system, the attenuation behavior of the Vibrometer accelerometer was then represented as a function of frequency by the classical amplification expression (Fig. 7a) that was used for correcting all high-frequency data obtained with the Vibrometer accelerometer. A second, relatively simple correction was necessary because of the use of analog low pass filters (2 kHz) to reduce signal aliasing (initially the frequency range of interest was 0–2000 Hz, but it was increased to 2500 Hz to capture the tip-resonance response behavior). The frequency roll-off characteristics (Fig. 7b shows individual and average behavior) were determined as part of the calibration activities of the charge amplifiers, and a correction equation was derived for the attenuation as a function of frequency.

Additional corrections became necessary due to the physical locations of the sensor elements being away from the far end of the thermowells. Since the various RTD simulants (accelerometer wands) were interchangeable, the sensor positions varied based on accelerometer type and monitoring direction. Fig. 7c shows the analytically determined deflection of the thermowell tip under static pressure loading that simulated the tip deflections due to turbulent buffeting. A similar, but different, deflection shape was computed for the dynamically responding thermowell tip. Thus, separate sets of correction factors were derived to extrapolate the measured amplitudes for those projected for the far ends of the thermowell tips. Fig. 7 shows these three forms of corrections in graphical form.

3.2. Thermowell tip-response test results

Separate sets of displacement PSD graphs were generated to determine the r.m.s. signal contents that could be attributed to turbulent buffeting and to tip-resonance response. Using spreadsheet manipulations, the data were corrected as necessary for filter attenuation, for accelerometer attenuation, and for sensor location. The results were then plotted in various fashions to allow for comparison and identification of major trends. Fig. 8 shows the adjusted turbulent buffeting and the adjusted tip-resonance responses as a function of flow velocity for the 121°C (250°F) loop condition. The following observations can be made:

- Turbulent buffeting responses in the lift direction are higher than in the drag direction.

[1] The term "turbulent buffeting" is used here to describe either broad band or narrow band tip responses forced far below the natural tip frequency due to organized turbulence embedded in the turbulent flow.

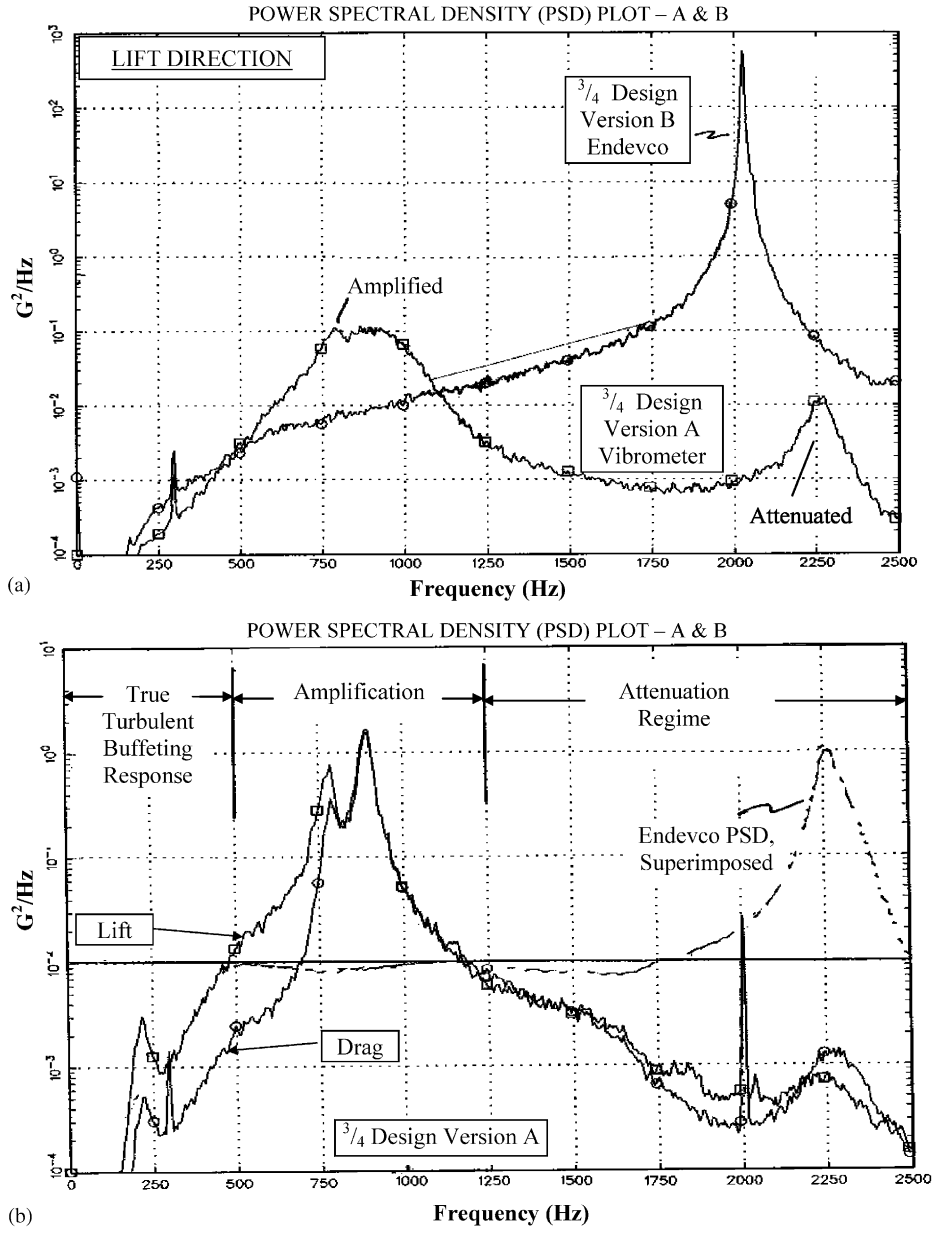

Fig. 5. Comparison of amplified/attenuated vibrometer accelerometer lift and drag PSDs with Endevco PSDs.

- Turbulent buffeting responses in the lift and drag directions of the Reference design and for the 3/4 design, Version A, are similar.
- Turbulent buffeting responses in the lift and drag direction of the longer Version B design are somewhat larger than those for the shorter free tip thermowell designs (Version A and Reference).
- Referring to Fig. 8b, it is seen that, for each design, lift axis and drag direction resonance response amplitudes are quite similar. However, the amplitudes for the longer Version B design are much larger.

Similar summary graphs were also generated for the 232°C and 316°C (450°F and 600°F) loop temperatures. Inasmuch as there were many similarities, not all test data were consistent. For example, during the first incremental test-series at 232°C (450°F), the tip response of the 3/4 thermowell Version B became very large and assumed an

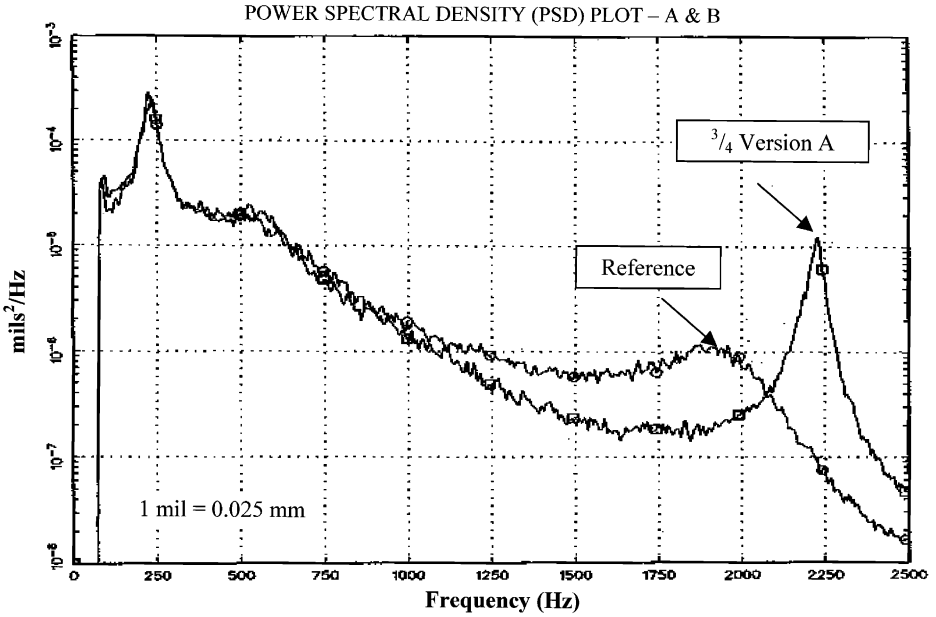

Fig. 6. Reference and 3/4 Version A thermowell designs, lift direction displacement PSD graphs.

"instability" type response at high flows. At that condition, there was also evidence of coupling with the adjacent thermowells, but at a relatively moderate level. Fig. 9 shows this instability behavior for a flow rate of 26.2 m/s (86 ft/s). It is also evident that here the tip-resonance response amplitude was higher than that due to turbulent buffeting which typically dominated the overall thermowell tip deflections. This behavior did not repeat itself, but effectively was the reason for not selecting that particular design. Referring in part to Fig. 10, several generalizations can be made. They are as follows:

- The Reference and the 3/4 Replacement design Version A had similar frequencies and similar response amplitudes.
- The scaled 3/4 Replacement design Version B always had lower frequencies and higher amplitudes than the Reference and the 3/4 Replacement Version A designs.
- The tip deflections attributed to turbulent buffeting were similar for all three designs. The lift direction components were typically higher than those in the drag direction.
- The tip deflections caused by turbulent buffeting were larger for the Reference and the Version A designs than those due to tip-resonance response. This was not always true for the Version B design due to its longer free length, which increased the tip-resonance response deflections more than the deflections attributed to turbulent buffeting.
- The measured tip frequencies fluctuated in a somewhat inconsistent fashion with temperature, and/or sensor configuration.

Fig. 11 shows a representative set of displacement time histories that also were used to generate companion orbital motion graphs. Such graphs were generated by double integration of the acceleration records, sampled at 25 kHz. The spreadsheet manipulations necessitated a variety of digital filtering processes including sliding "low pass" and, in the case of the Vibrometer accelerometer, also sliding "notch" filtering in order to eliminate the internal accelerometer biases, and to apply separate corrections for the turbulent buffeting and the resonance response motion components. The time histories reflect broad and/or narrow band random motion behavior and the signal amplitudes agree with those derived from the spectral data. The orbital motions are slightly elliptical. Despite the very high sampling rate of 25 kHz, the traces are somewhat rough.

Whereas most data were obtained from the incremental flow sweep testing, 30-min records for continuous flow sweep runs were also obtained for all test conditions. These runs resulted in very large data files ($\sim$400 Mb) and, for each signal channel, needed to be processed in eight to ten separate waterfall plots, each limited to 1000 spectral analyses. Selective processing demonstrated that there was no other FIV phenomena. The Waterfall plots only exhibited the reported amplitude increases with flow.

During testing at 232°C (450°F), two of the four Endevco accelerometers failed. The remaining two experienced deterioration of sensitivity. Based on post-test calibrations, the data recorded further into that test-series were corrected

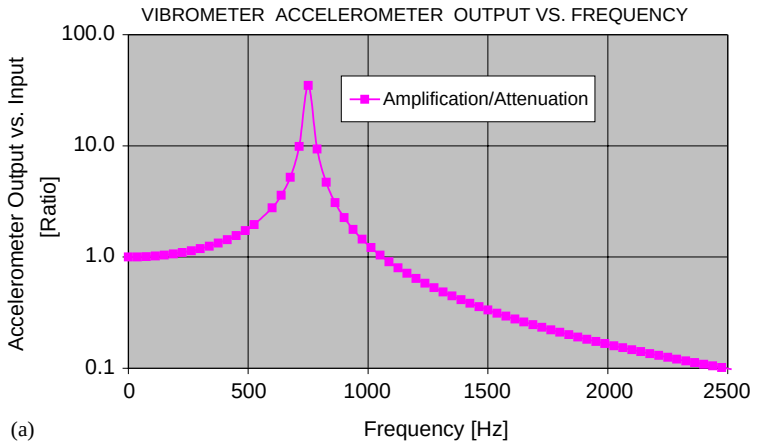

(a)

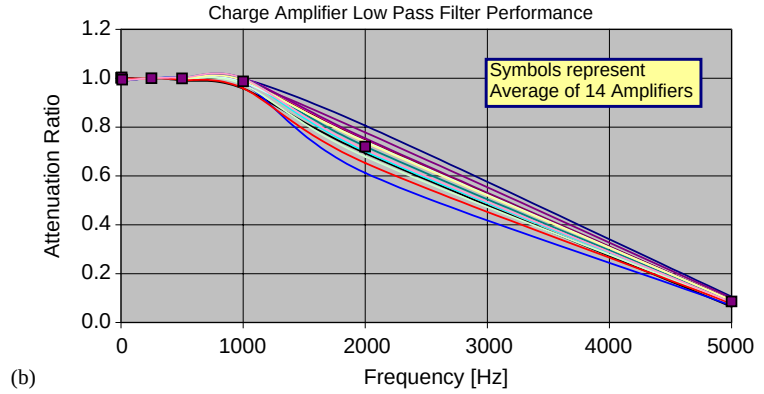

(b)

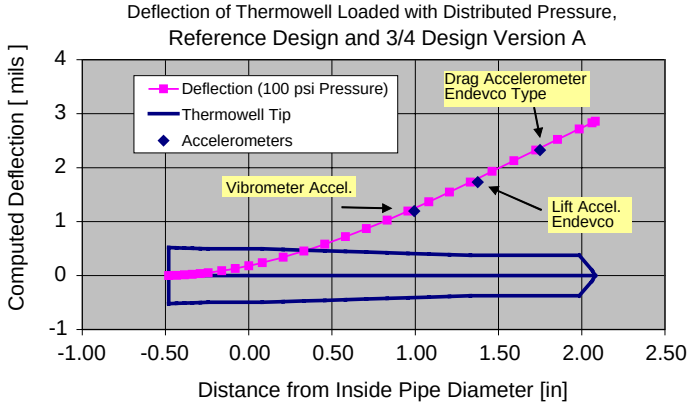

(c)

Fig. 7. RTD thermowell tip motion correction factors.

accordingly. Most disturbing, however, was the failure of the high temperature Vibrometer accelerometer in fatigue. It must be realized that, while the measured tip deflection amplitudes were typically less than a fraction of a mil, the associated acceleration values exceeded 300 Gs. As a result of these issues, a considerable effort was required to sort through the available test data and to apply the proper corrections. At that time it was decided to assemble a new high temperature accelerometer for use at 316°C (600°F) and also several low temperature Endevco units for repeat testing at 121°C (250°F). Since only one accelerometer wand was available for high temperature testing, the three thermowell designs were tested in sequence. Since, for this high test temperature, no set of comparison data was available, the "low temperature" correction processes were applied. They consisted of adjusting the turbulent buffeting measurements for sensor location. The tip-resonance responses were adjusted by applying all three correction factors.

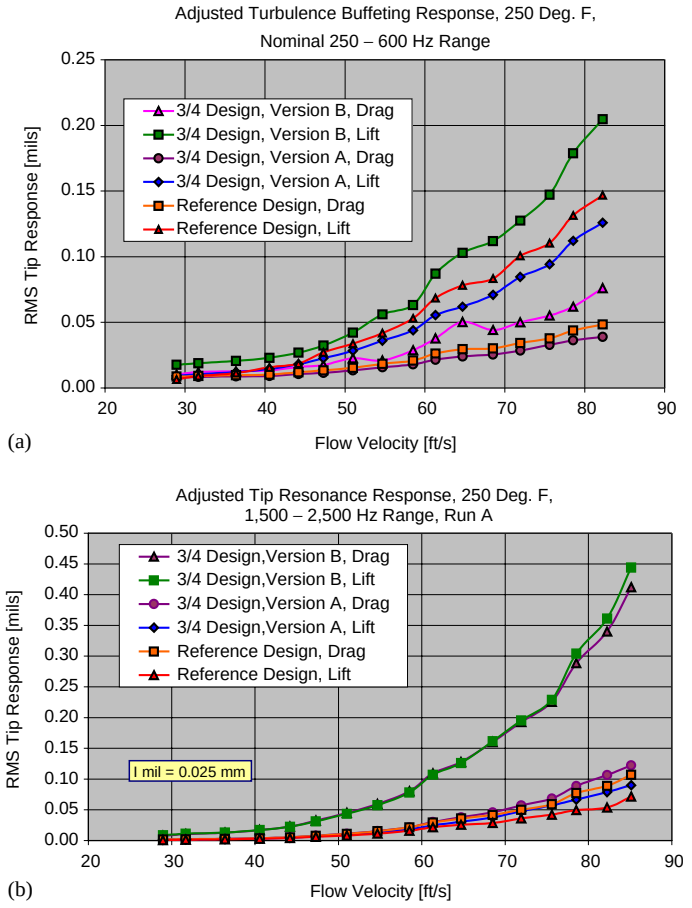

Fig. 8. R.m.s. Lift axis and drag axis responses 121°C (250°F), all designs.

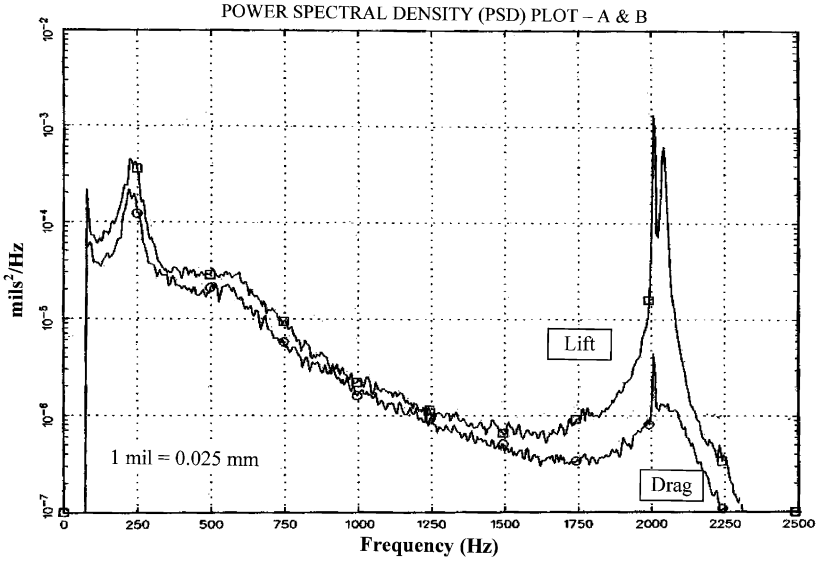

Fig. 9. Instability displacement PSD graph for $\frac{3}{4}$ design Version B.

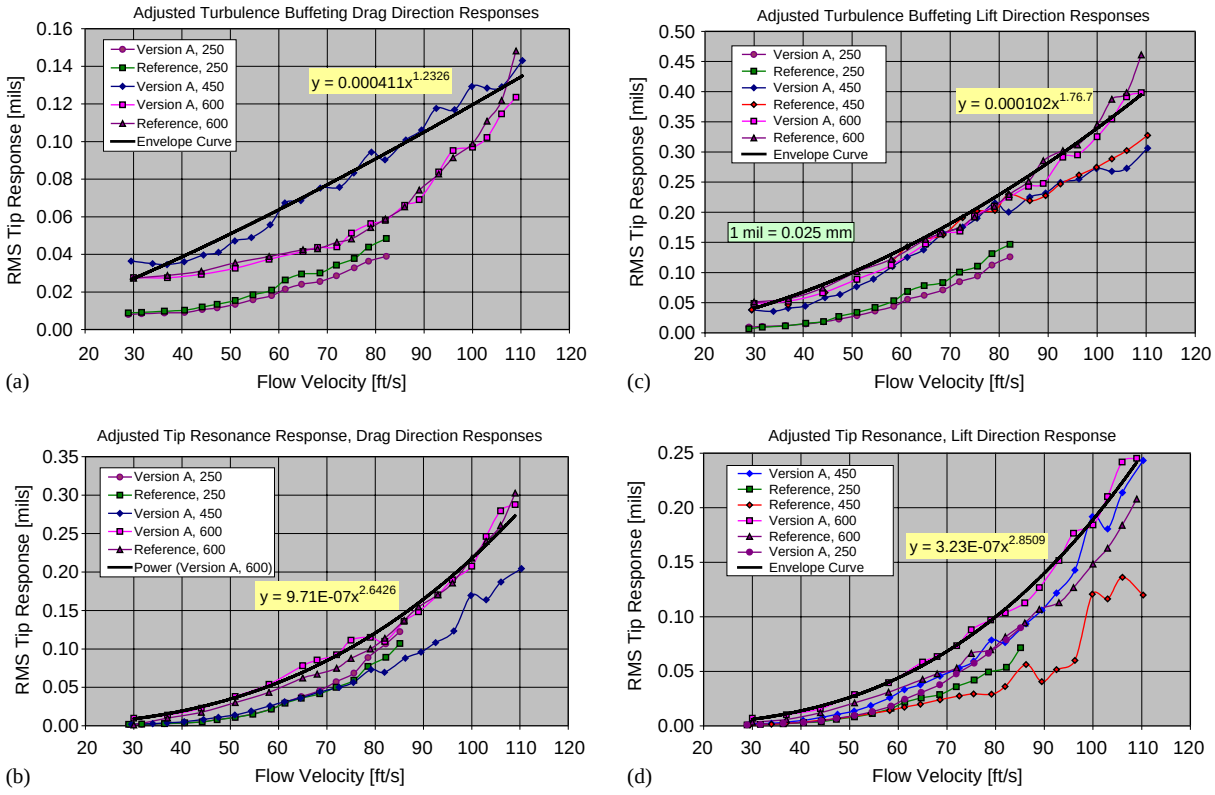

Fig. 10. Results for $\frac{3}{4}$ designs, Version A and reference design.

Despite all these efforts, some inconsistencies remain in the data trends for the three test temperatures. Also, while the data for each condition could have been curve-fitted by normalizing the data with respect to dynamic head, no uniform expression could be derived that suited all sets of results. Therefore, because of the similarity in behavior, results for the Reference design and for the Version A design were combined and treated separately from the Version B design. Referring to Fig. 10, the lift and the drag responses due to both turbulent buffeting and tip-resonance response are shown on separate plots, but with superposition of the results from all three temperature conditions. The data curves in each graph are represented by single envelope expressions. For convenience, the power expressions were converted into equivalent single-term quadratic expressions that are further combined into separate Root-Sum-of-the-Squares (RSS) expressions (as a function of flow) for turbulent buffeting and tip-resonance response. Resorting to the earlier mentioned analyses for deflections shapes due to quasi-static loading and dynamic tip response, separate relationships were available to translate the two types of tip deflections to thermowell base bending moments, and thus to base bending stress. Since both the broad band turbulent buffeting and the narrow band tip-resonance response motions reflected Gaussian distributions, the peak stress levels were thus available in empirical form as a function of flow rate and could be used directly in the stress analysis in place of the original, theoretical considerations that were based solely on vortex shedding considerations, which these test results did not demonstrate to be applicable.

Fig. 12 summarizes the thermowell "Deflection and Stress Design Curves" that were used in the stress analysis. The Version B design data is also included and the previously mentioned instability behavior is reflected in the data trend above 24.4 m/s (80 ft/s) flow velocity. Since the actual design flow velocity for the intended "Hot-Leg" RTD thermowell/nozzle replacements is only 24.6 m/s (80.8 ft/s) compared with 33.5 m/s (110 ft/s) for the "Cold-Leg" RTDs, and since actual normal operating Hot-Leg flow rates are less than 19.8 m/s (65 ft/s), a considerable margin of safety against fatigue was demonstrated.

Evaluation of the test-section and the RTD head accelerometers demonstrated that the overall loop vibration levels and the RTD head motions were quite small and thus considered negligible.

The qualification testing of the new thermowell designs also included endurance flow testing at 316°C (600°F) with 70 h at 24.4 m/s (80 ft/s) flow velocity and with 48 h at 26.2 m/s (86 ft/s) flow velocity. The number of vibration cycles that were accumulated during this duty test exceeded those typically associated with "infinite life" by a factor of 80.

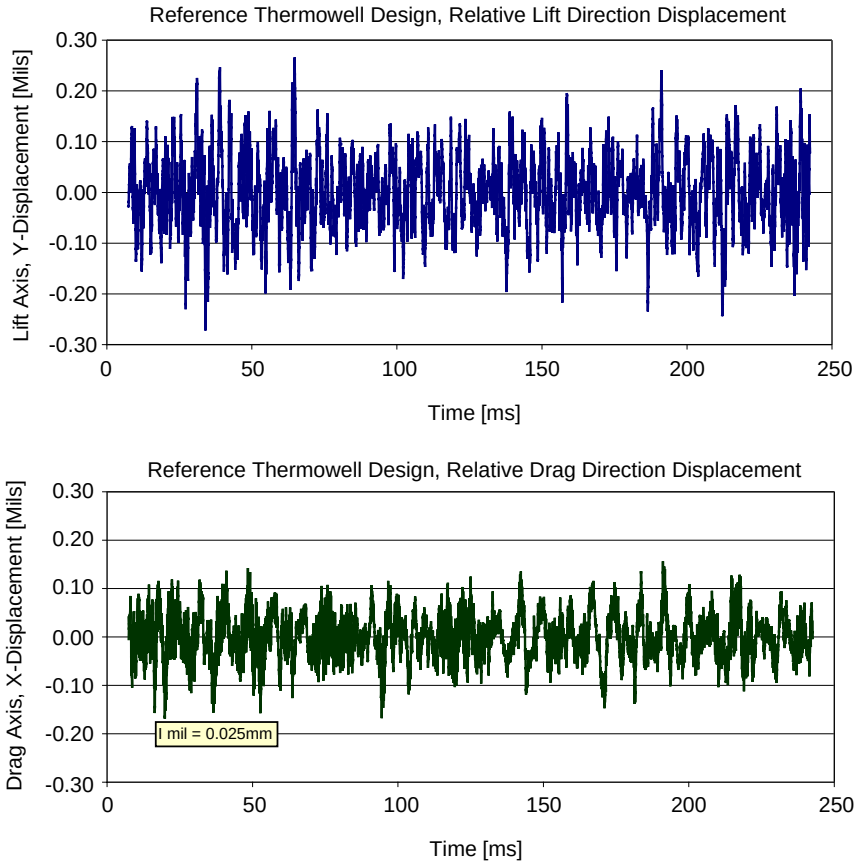

Fig. 11. Representative displacement time histories.

Post-test inspections did not reveal any wear marks or any evidence that could have been associated with fretting and/or fatigue.

3.3. Turbulent buffeting peak response frequency and amplitude

In addition to completing a successful qualification program for a new 3/4 Replacement Thermowell Design for the sponsoring utility, the test data offers information of more general interest. In comparison with tests performed on a variety of other components, the subject test is unusual since its results cover an extremely wide range of frequencies (0–2500 Hz). This wide test range was a deliberate choice, because of both low- and high-frequency response contributions (selected spectrum analyses up to 10 kHz demonstrated no significant responses above 2.5 kHz). As mentioned above, the absence of any detectable vortex-shedding-induced response (in the true classical sense) was somewhat of a surprise. Empirical expressions were derived that define the turbulent buffeting, Blevins (1977), and the tip-resonance responses as functions of flow velocity squared. A distinct peak that increases in amplitude with flow velocity squared dominates the turbulence buffeting response. The frequency of the peak increases proportionally with velocity. Although this may only be a coincidence, the peak frequency compares favorably to a predicted vortex shedding frequency if one uses a turbulence-based Strouhal number of 0.45 in combination with the free thermowell tip length of 54 mm (2.125 in), rather than the diameter of 9.53–12.7 mm (0.375–0.50 in). The following expressions define the observations made for a temperature of 316°C (600°F):

$$\text{Peak-frequency (Hz)} = 7.83 \times V;$$
$$\text{R.m.s. drag amplitude (mm)} = 8.8 \times 10^{-6} \times V^2;$$
$$\text{R.m.s. lift amplitude (mm)} = 2.4 \times 10^{-6} \times V^2;$$

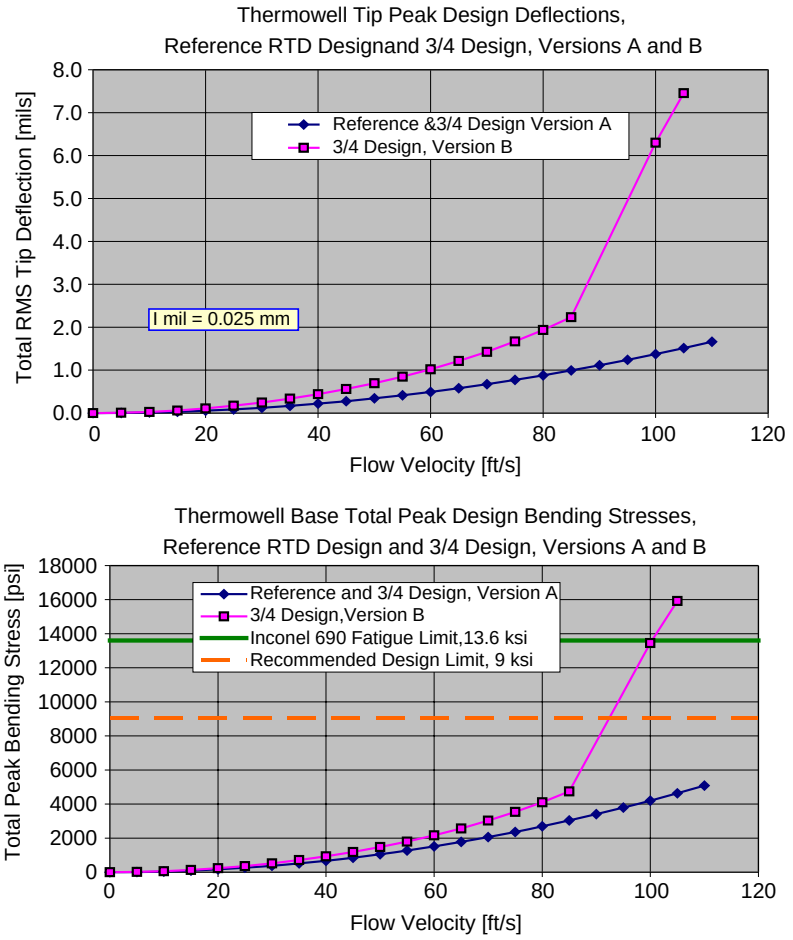

Fig. 12. Thermowell design deflections and design stresses as a function of flow velocity.

where cross-flow velocity is in units of m/s. Also, an assumed, uniform pressure of 1 MPa across the thermowell tip area exposed to cross-flow results in 0.105 mm tip deflection.

In an effort to use these results as a design tool, an Effective Force Coefficient is derived using the following expression:

$$F = CA\rho V^2/2\,g.$$

Applying the empirical data, the Effective Lift Coefficient C_l is determined as 0.223 and the Effective Drag Coefficient C_d as 0.057. It is interesting to note that Walshe (1962) reported a lift coefficient of 0.230 for the observed amplitude range.

3.4. Tip-resonance response, dimensionless turbulence force spectra

Methodologies involved in the determination of dimensionless turbulence force spectra from experimental results on tubular arrays have been documented by Axisa et al. (1990) and Haslinger and Steininger (1995). Using turbulence response measurements at a particular location, the knowledge of the mode shape, an estimate of the flow velocity distribution along the structure, the dimensional properties, the turbulence correlation length, the structural natural frequency and damping, combined with theoretical considerations for the response of a structure due to turbulence excitation, an expression for determination of nondimensional forcing functions, per unit length, may be written as

$$\Phi_F = \left[\frac{\sigma_n(s)8\pi^{3/2}M_n f_n^2}{1/2\rho\overline{V_g}^2 D\delta_n(s)L_{cn}}\right]^2 \frac{\zeta_n}{f_r}.$$

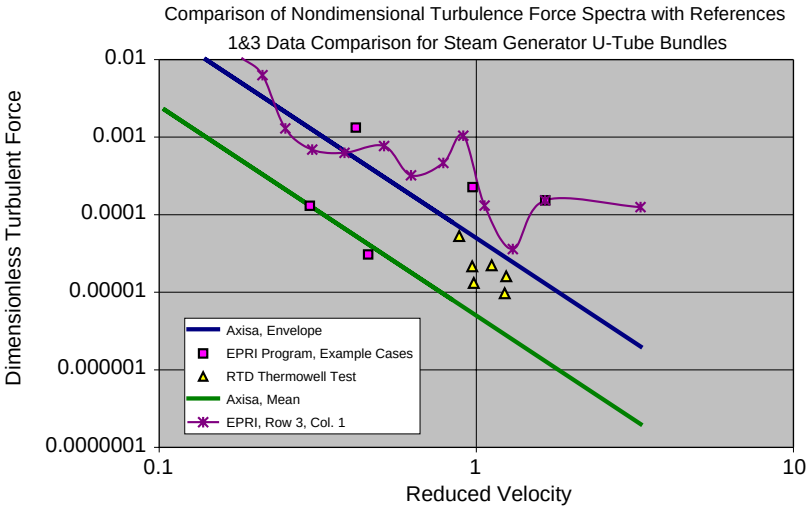

Fig. 13. Nondimensional turbulence force vs. reduced velocity, RTD/thermowell response comparison with literature data.

Table 1
RTD flow test program, drag direction example cases for 121°C (250°F), all three test designs

Test temperature Thermowell design Flow velocity (ft/s)	Units	121°F Reference 68	121°F 3/4 Version A 68	121°F 3/4 Version B 68	121°F Reference 68	121°F 3/4 Version A 68	121°F 3/4 Version B 68
Tube diameter	(mm)	11.43	11.43	11.43	11.43	11.43	11.43
Fluid density	(kg/m^3)	950	950	950	950	950	950
Approach (gap) velocity	(m/s)	20.7	20.7	20.7	26.2	26.2	26.2
Thermowell frequency	(Hz)	2225	2250	2025	2225	2250	2025
General correlation length	(m)	0.0484	0.0484	0.0484	0.0484	0.0484	0.0484
Critical damping	(dimensionless)	0.0160	0.0210	0.0033	0.0124	0.0085	0.0206
Generalized mass	(dimensionless)	0.0134	0.0134	0.0134	0.0134	0.0134	0.0134
Relative modal deflection	(dimensionless)	0.856	0.856	0.856	0.856	0.856	0.856
R.m.s. displacement	(mm)	0.0009	0.0010	0.0034	0.021	0.0023	0.0095
Dim. turbulent force	(dimensionless)	9.70E−06	1.60E−05	2.23E−05	2.16E−05	1.32E−05	5.29E−05
Reduced velocity	(dimensionless)	1.229	1.242	1.118	0.971	0.982	0.883

Application of this methodology requires that the structure response due to turbulence occurs at discrete frequencies for which the modal, narrow-band r.m.s. responses are determined. Several thermowell cases were evaluated and are compared in Fig. 13 to the five example cases reported by Haslinger and Steininger (1995), as well as to the upper limit and mean expressions suggested by Axisa et al. (1990). Table 1 lists all pertinent parameters for the thermowell cases. The corresponding parameters for the comparison U-tube example cases are those reported by Haslinger and Steininger (1995).

The agreement of the nondimensional force spectrum values, derived for representative sets of thermowell tip-resonance responses, with the referenced results for steam generator U-tube arrays was surprising since the latter have significantly lower response frequencies (<150 Hz). This would suggest that the nondimensional turbulent forcing functions for short, isolated cantilevered structures with high natural frequencies under high velocity turbulent environments may also be predicted by the referenced data.

4. Conclusions

Extensive qualification testing was performed on a new 3/4 thermowell replacement design up to 136% of cold leg and 175% of hot leg flow velocities, and at temperatures ranging from 121°C to 316°C (250–600°F). The new design

compared favorably with the current design that has been in operation for almost 20 years in three plants. There was no observation of any vortex-shedding-induced thermowell response. Failures in earlier thermowell designs had been attributed to this mechanism. Thermowell tip responses were attributed to turbulent buffeting between 100 and 600 Hz and to tip-resonance frequencies at 2000 Hz and above, which were being excited by broad band turbulence. The acceleration measurements were interpreted in terms of tip deflections, and resulting stress levels were found to be well below the fatigue allowable, as further demonstrated by successful completion of an extensive endurance test phase.

Acknowledgements

The author would like to thank Messers A. Meeden and R. Yuhaz of the Arizona Public Service Co. (APS) and Mr D. Siska from Westinghouse for their contributions during the design and testing phases of this program. APS also provided the financial sponsorship for this program.

References

Axisa, F., Antunes, J., Villard, B., 1990. Random excitation of heat exchanger tubes by cross-flows. Journal of Fluids and Structures 4, 321–341.

Blevins, R.D., 1977. Flow-Induced Vibration. Van Nostrand Reinhold Co, New York.

Haslinger, K.H., Steininger, D.A., 1995. Vibration response of a U-tube bundle with anti-vibration bar supports due to turbulence and fluidelastic excitations. Journal of Fluids and Structures 8, 805–834.

Walshe, D.E., 1962. Some measurements of the excitation due to vortex shedding of a smooth cylinder of circular cross section, National Physical Laboratory Aero Report 1062.